





Dynamic response characteristics of dry and water-saturated schist under impact loading

ZHOU Yang¹  <https://orcid.org/0000-0001-9624-973X>; e-mail: 2016026017@chd.edu.cn

SU Sheng-rui^{1*}  <https://orcid.org/0000-0003-0905-8869>;  e-mail: shengruisu@163.com

CHEN Jian-xun²  <https://orcid.org/0000-0001-8672-5114>; e-mail: chenjx1969@chd.edu.cn

*Corresponding author

¹ School of Geological Engineering and Geomatics, Chang'an University, Xi'an 710064, China

² School of Highway, Chang'an University, Xi'an 710064, China

Citation: Zhou Y, Su SR, Chen JX (2020) Dynamic response characteristics of dry and water-saturated schist under impact loading. *Journal of Mountain Science* 17(12). <https://doi.org/10.1007/s11629-019-5900-2>

© Science Press, Institute of Mountain Hazards and Environment, CAS and Springer-Verlag GmbH Germany, part of Springer Nature 2020

Abstract: Many geological engineering hazards are closely related to the dynamic mechanical properties of rock materials. However, most existing studies on the dynamic mechanical properties of rock materials were conducted on the hard rocks such as sandstone, granite, limestone, and marble, whereas soft rocks, such as schist, are less studied. Therefore, in this study, a series of triaxial impact tests were conducted on dry and saturated schist by employing a modified triaxial split Hopkinson pressure bar system to reveal the coupling effects of water, strain rate, and triaxial confining pressure on the mechanical properties of schist. The results show that schist is a type of water-sensitive rock and the stress-strain curve of saturated schist has apparent ductility. The effects of strain rate on dynamic strain, deformation modulus and peak stress were analyzed. The results also show that the dynamic peak stress is affected by the combined softening effect and viscous effect of water under impact loading. Finally, it was found that the failure mode of schist belongs to typical axial tensile failure under uniaxial impact tests, and shear failure is the main failure mode under triaxial impact tests. With the increase in confining pressure, the failure modes

of schist change from tensile failure to shear failure. This research can provide useful parameters for geological engineering hazard prevention in mountain areas.

Keywords: Dry and water-saturated schist; Triaxial stress constraint; Modified triaxial split Hopkinson pressure bar; Dynamic mechanical behavior; Impact loading

Introduction

Soft rock has always been the focus of engineering geology (Aydan et al. 2014; Chen et al. 2017), paying specific attention to the significant effect that water has on the mechanical properties of rock materials. Mechanical properties of water-saturated rock are closely related to the stability of engineering rock mass. Although static mechanical properties of saturated rock have been studied (Vásárhelyi and Ván2006; Erguler and Ulusay 2009; Karakul and Ulusay 2013; Roy et al. 2017; Wong et al. 2018), in engineering activities, engineering rock mass is often affected by dynamic loads such as earthquakes, mechanized construction, and blasting. Consequently, many

Received: 13-Nov-2019
1st Revision: 04-Feb-2020
2nd Revision: 09-May-2020
Accepted: 11-Jun-2020

geological engineering hazards (such as foundation deformation and slope instability) are closely related to the dynamic mechanical properties of rock materials (He et al. 2005; Zhou et al. 2018). Therefore, it is insufficient to study the static mechanical property of saturated rock; in recent years, some progress has been achieved in studying its dynamic mechanical properties as well. Such studies found that saturated rock has high compressive strength because of the Stefan effect (Zhang and Zhao 2014). However, most of these studies were focused on hard rocks such as sandstone (Huang et al. 2010; Wang et al. 2010; Zhou et al. 2016; Zhou et al. 2019), granite (Lou 1994), limestone (Petrov et al. 2017), and marble (Gao et al. 2018). Few studies addressed soft rocks such as schist, a typical soft rock widely distributed on the surface of the earth containing many clay minerals. As schist demonstrates strain softening behavior when absorbing water, water-rock interaction cannot be ignored in its mechanical analysis.

In previous studies, uniaxial compression, tensile, and fracture tests have been carried out on the rock samples (Huang et al. 2010; Lou 1994; Petrov et al. 2017; Wang et al. 2010; Zhou et al. 2016; Zhou et al. 2019). The obtained results have greatly promoted the development of rock dynamics; however, the effect of crustal stress on the dynamic mechanical properties of saturated rock was not considered. Nonetheless, in engineering activities, saturated rock is affected by the combined triaxial confining pressure and dynamic load. At present, the dynamic mechanical properties of saturated rock under triaxial stress constraints are not clear. Hence, to prevent and control geological hazards and protect the ecological environment in mountainous areas, studying the coupling effects of triaxial confining pressure, water, and dynamic load on the mechanical behavior of soft rocks is necessary.

With this in mind, in this study, we have carried out a series of triaxial impact tests on dry and water-saturated schist by employing a modified triaxial split Hopkinson pressure bar (SHPB) system. For comparison, we also conducted static triaxial compression tests. The modified triaxial SHPB system was selected as it can provide constant triaxial confining pressure for rock samples before applying dynamic loads. In

addition, we analyzed the coupling effects of strain rate, water, and triaxial confining pressure on mechanical properties of schist and the dynamic response mechanism of saturated schist was revealed. We believe that this work can provide useful parameters for geological hazard prevention in mountain areas.

1 Test Materials and Scheme

1.1 Materials

In this study, we used weakly weathered schist obtained from northwest Wenchuan county, where Silurian and Ordovician strata are mainly found in this area, in Sichuan province, China (Appendix 1). Wenchuan county in China is among the regions most affected by serious engineering geological hazards. The rock mass is distributed in layers. There are a series of metamorphic rocks in this area, mainly schist, phyllite, and metamorphic sandstone. A slope with interbeddings of soft and hard layers is the main type in this area. The engineering geological properties of soft and hard rocks are quite different from each other. In the construction of highways, tunnels and slope engineering, the safety and stability of construction projects are seriously affected by the mechanical properties of soft rock. Under external loads (such as mechanized construction and blasting), slope instability and chamber collapse occur frequently. Therefore, in this study, the schist with the lowest strength and the greatest impact on the stability of the project was selected as the study material. The rock blocks with good integrity were selected on the slope surface to be processed into rock samples. The sample was composed of quartz (32%), albite (8%), muscovite (38%), and chlorite (22%), with average density and P-wave velocity amounting to 2.82 g/cm³ and 2.08 km/s, respectively. Furthermore, average porosity and saturated water content amounted to 2.23% and 0.81%, respectively.

1.2 Sample preparation

According to the recommendations of the International society of rock mechanics (ISRM) for rock dynamic tests, the schist was processed into

Ø50 mm × 25 mm cylindrical samples. In addition, the Ø50 mm × 100 mm cylindrical samples were used for static tests by employing the RMT-150C (a rock mechanics test system). The schist has obvious schistosity. The schistosity plane of rock specimen is nearly horizontal (Appendix 2). The two ends of the samples were polished. P-wave velocities and densities of all samples were measured to remove the outliers. Selected samples were placed in an oven with a constant temperature of 105 °C until the mass was constant. At that time, the samples were considered to be dry. Half of the dry samples were first vacuumed for 8 h using vacuum pumping and then placed in an aqueous solution for 48 h; after this, the samples were considered to be saturated. Before testing, the water-saturated samples were placed in fresh-keeping bags to prevent water evaporation. Sample preparation and test equipment are shown in Appendix 3.

1.3 Test equipment and procedure

A series of impact tests were carried out using the modified triaxial SHPB. This equipment can eliminate the high frequency oscillations and generate well-repeatable half-sine waves (Li et al. 2005; Zhou et al. 2011; Li et al. 2014). Compared with the conventional SHPB, the modified triaxial SHPB includes the active axial pressure device and active confining pressure device (Appendix 4). Therefore, the static triaxial pre-stress can be applied before impact loading. The detailed parameters of the modified triaxial SHPB can be found in related literature (Gong et al. 2011). The impact tests consist of two parts: uniaxial and triaxial impact tests. In the triaxial impact test, the pre-stressed loading system and the impact loading system were independent. Before impact loading, triaxial confining pressures were applied to the predetermined levels (5 and 10 MPa). The dynamic stress-strain curves can be obtained using Eqs. (1) - (3). In the static compression test, the axial stress was applied to the schist at a constant strain rate (10⁻⁵ s⁻¹) until failure. In this paper, the static and dynamic tests of schist samples were carried out under drained conditions.

Based on the one-dimensional stress wave theory, the wave signals collected by the strain gauges attached to the incident and transmission

bars can be used to calculate the stress, strain, and strain rate of the specimens using Eqs. (1) - (3) (Zhou et al. 2012; Zhou et al. 2016).

$$\sigma(t) = \frac{A_c E_c}{2A_s} [\varepsilon_1(t) + \varepsilon_R(t) + \varepsilon_T(t)] \quad (1)$$

$$\varepsilon(t) = \frac{C_c}{L_s} \int_0^t [\varepsilon_1(t) - \varepsilon_R(t) - \varepsilon_T(t)] dt \quad (2)$$

$$\dot{\varepsilon}(t) = \frac{C_c}{L_s} [\varepsilon_1(t) - \varepsilon_R(t) - \varepsilon_T(t)] \quad (3)$$

where $\sigma(t)$, $\varepsilon(t)$ and $\dot{\varepsilon}(t)$ are the stress, strain and strain rate of rock at a certain moment t , respectively; $\varepsilon_1(t)$, $\varepsilon_R(t)$ and $\varepsilon_T(t)$ are the incident strain, reflected strain and transmitted strain at a certain moment t , respectively; A_c , E_c and C_c are the cross-sectional area, elastic modulus and wave velocity of the elastic rod, respectively; A_s and L_s are the cross-sectional area and length of specimen, respectively.

2 Test results and analysis

The strain rate, peak strain, peak stress, and deformation moduli of saturated and dry schist under different confining pressures are shown in Appendix 5 (strain rate varies from 96 to 262 s⁻¹).

2.1 Analysis of strain rate and confining pressure effects

2.1.1 Stress-strain curve

The dynamic stress-strain curves of saturated and dry schist (shown in the Figures 1-3) shifted to the right with the increase of strain rate. As shown in Figure 4, OA, AB, BC, and CD are the compaction, elastic, plastic deformation, and failure segments. The compaction segments of saturated and dry schist are not clearly visible, which may be related to the sample sizes. Furthermore, water has a significant effect on the stress-strain curve (Figure 4a). When the strain rates are approximately the same, plastic strain of saturated schist is larger than that of dry schist (Appendix 6). Owing to the softening effect of water, the water-saturated schist has a long BC segment. Near the peak stress, yield platforms

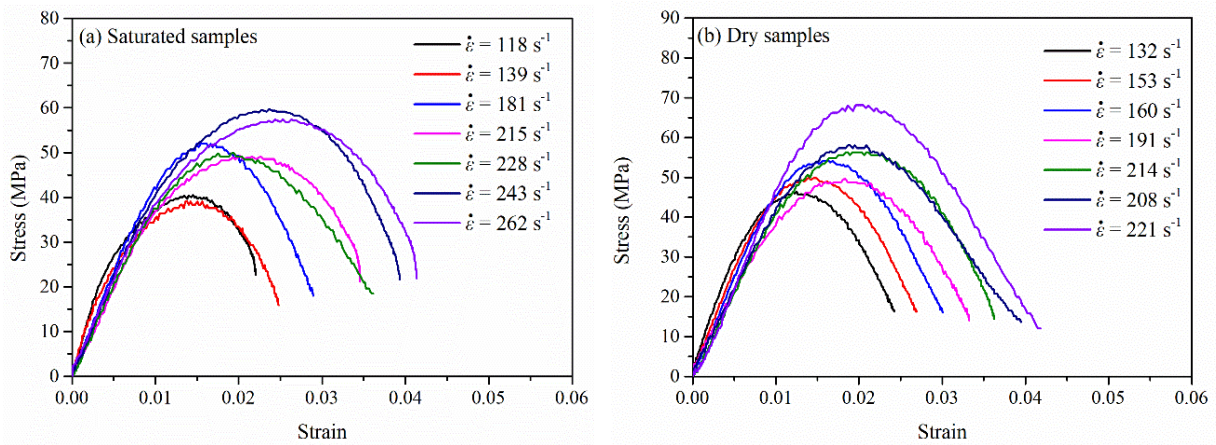


Figure 1 Uniaxial dynamic stress-strain curves: (a) Saturated samples; (b) Dry samples. $\dot{\epsilon}$ is the strain rate.

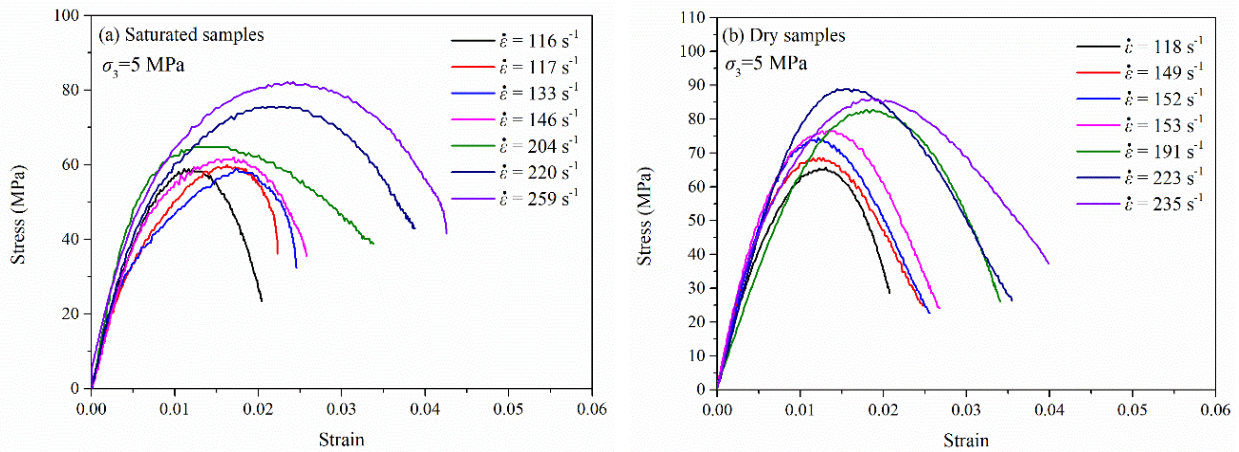


Figure 2 Triaxial dynamic stress-strain curves: (a) Saturated samples; (b) Dry samples. Confining pressure σ_3 is 5 MPa; $\dot{\epsilon}$ is the strain rate.

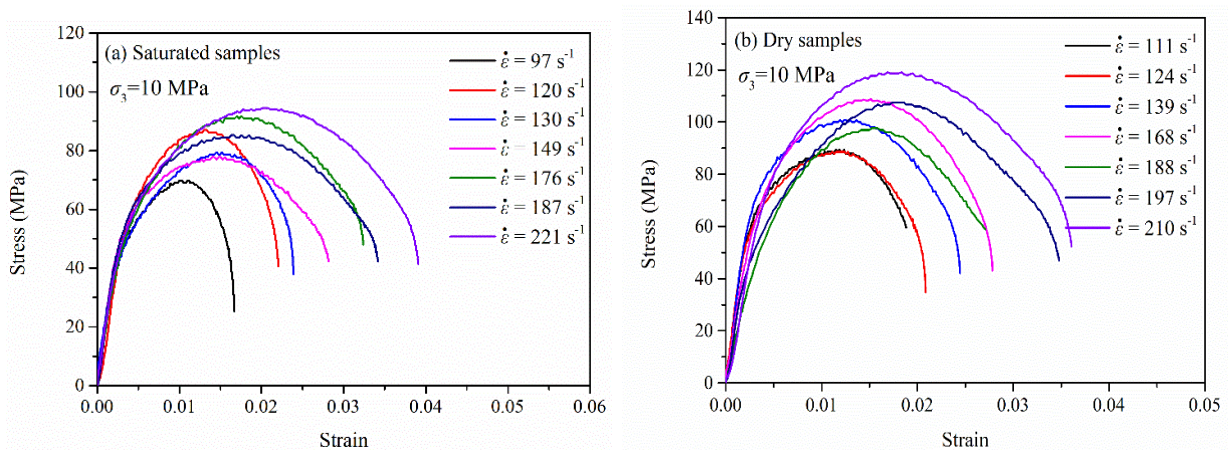


Figure 3 Triaxial dynamic stress-strain curves: (a) Saturated samples; (b) Dry samples. Confining pressure σ_3 is 10 MPa; $\dot{\epsilon}$ is the strain rate.

appear on the stress-strain curves of saturated schist, which implies that the saturated schist has clear ductility. In addition, the saturated curve is relatively full and the lower opening is larger,

whereas the drying curve is relatively narrow. The confining pressure also has an effect on the stress-strain curve (Figure 4b). With the increase in confining pressure, the slope of the AB segment

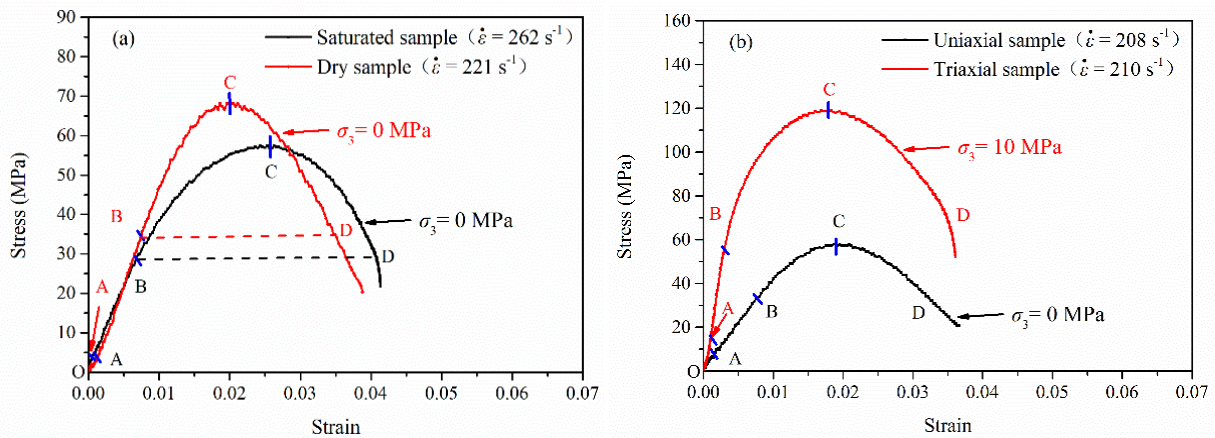


Figure 4 Segment division of typical stress-strain curves: (a) Segment division of uniaxial stress-strain curves; (b) Segment division of uniaxial and triaxial stress-strain curves. $\dot{\epsilon}$ is the strain rate. σ_3 is the confining pressure.

increases and the ability of schist to resist deformation is improved.

2.1.2 Dynamic strain

In this paper, some parameters were defined to evaluate the deformation behavior of schist (Figure 5). The x-coordinate point corresponding to dynamic peak stress on stress-strain curve was defined as the dynamic peak strain (ϵ_d). As shown in Figure 4, the compaction segment (OA segment) is very small in the stress-strain curve. Therefore, the pre-peak curve can be roughly divided into two stages: OB and BC segments. The OB segment is approximately elastic. For convenience, the x-coordinate point corresponding to point B on stress-strain curve was defined as the dynamic elastic strain (ϵ_e). The difference between peak strain (ϵ_d) and elastic strain (ϵ_e) was defined as the dynamic plastic strain (ϵ_p). In addition, in order to make the test data more comparable, the deformation moduli at specific strain levels (E_1^d and E_2^d) have been added. E_1^d is the secant modulus of schist. E_2^d is the peak-state deformation modulus of schist.

$$E_1^d = \frac{\sigma_{50}}{\epsilon_{50}} \quad (4)$$

$$E_2^d = \frac{\sigma_d}{\epsilon_d} \quad (5)$$

where σ_d is the peak stress; ϵ_d is peak strain; σ_{50} is the stress value that is at 50% of the peak stress; ϵ_{50} is the axial strain corresponding to σ_{50} .

The dynamic strain is an important indicator for evaluating deformation and failure of rock

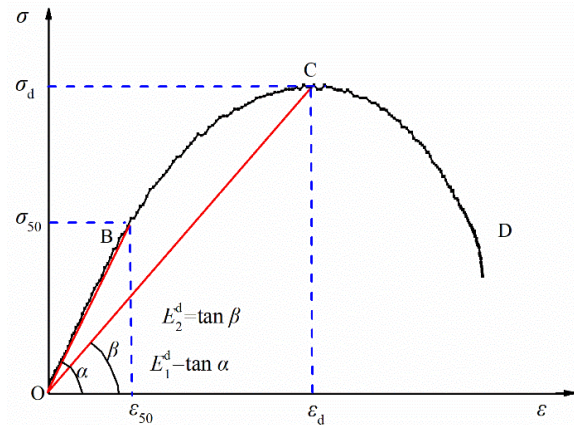


Figure 5 Sketch of definition method of deformation modulus. E_1^d is the secant modulus; E_2^d is the peak-state deformation modulus; σ_d is the peak stress; ϵ_d is peak strain; σ_{50} is the stress value that is at 50% of the peak stress; ϵ_{50} is the axial strain corresponding to σ_{50} .

materials (Gong et al. 2019). Figure 6 shows that the peak strain (ϵ_d) increases with increasing strain rate. When the strain rates are approximately the same, the peak strains of water-saturated schist are larger than those of dry schist. In addition, the peak strain shows no clear relationship with the increasing confining pressure (Figure 6).

The variation in schist peak strain with strain rate and confining pressure is fundamentally the same as in the previous results (Gong et al. 2019; Wang et al. 2018). However, when the sample sizes are the same, the peak strain of schist is larger than that of granite (Figure 7). The peak strain of schist is in the range of 0.0115-0.0151 (strain rate varies from 111 to 168 s^{-1}), whereas that of granite is in the range of 0.0073-0.0088 (strain rate varies from 114 to 142 s^{-1}). Hence, the peak strain of schist is almost twice as that of granite. The dynamic plastic

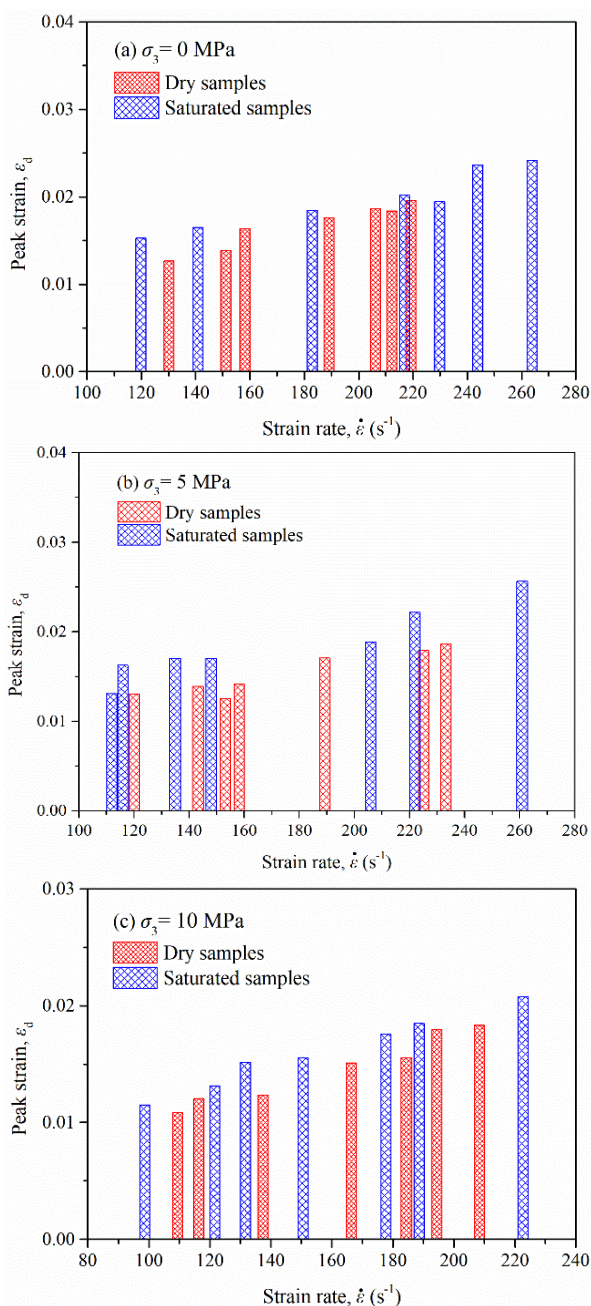


Figure 6 Dynamic peak strains of schist under different strain rates. σ_3 is the confining pressure.

deformation of schist is larger than that of granite when the sample sizes are the same. This phenomenon may be related to the mineral composition of rocks. There is a considerable amount of clay minerals in schist. The ability of clay minerals to resist deformation is weak. When the strain rates are approximately the same, the deformation of schist is greater than that of granite. In addition, the compaction segments of granite are not easily detectable and confining pressure has

a clear effect on its deformation. When the confining pressure is 10 MPa, post-peak curves of granite show a clear strain softening behavior.

2.1.3 Dynamic modulus

Figures 8 and 9 show the variation in deformation moduli (E_1^d and E_2^d) of dry and saturated schist with strain rate and confining pressure. It can be found that E_1^d and E_2^d increase with the increase of confining pressure. Even though the peak strain of schist is not sensitive to the confining pressure (Figure 6), the peak stress of schist increases with the increase of confining pressure. Therefore, with the increase in confining pressure, deformation moduli increase and the ability of schist to resist deformation increases. When the strain rates are approximately the same, the deformation moduli (E_1^d and E_2^d) of saturated schist are lower than those of dry schist. Hence, compared with the dry schist, the ability of saturated schist to resist deformation is weakened. However, E_1^d and E_2^d are not sensitive to the strain rate. Although test data are discrete, the deformation moduli are basically independent of the strain rate.

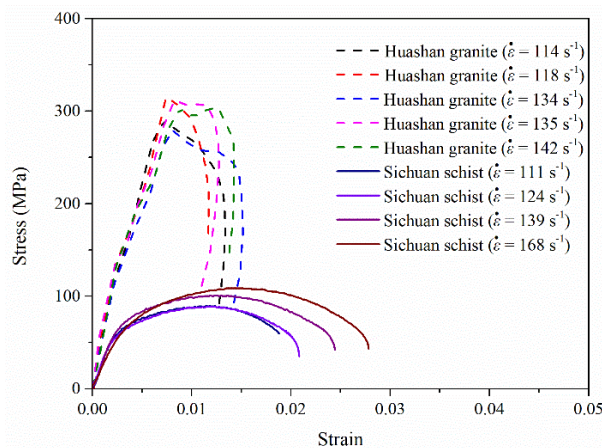


Figure 7 Comparison of triaxial stress-strain curves between schist and granite (The data of Huashan granite are from Wang et al. (2018)). Confining pressure σ_3 is 10 MPa; $\dot{\epsilon}$ is the strain rate.

2.1.4 Dynamic peak stress

The dynamic peak stress of saturated schist is lower than that of dry schist (Figure 10). Furthermore, with the increase in confining pressure, dynamic peak stress increases linearly. The peak stress increases with increasing strain rate. To study the relationship between dynamic

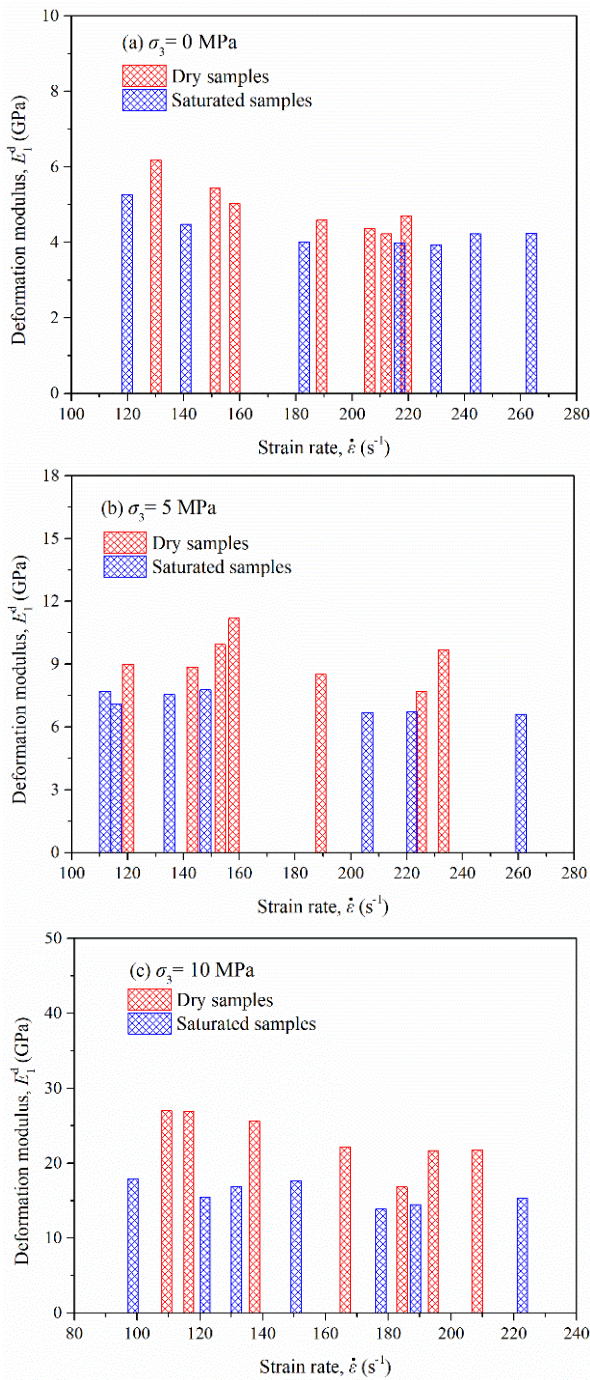


Figure 8 Relationship between dynamic deformation modulus (E_1^d) and strain rate. σ_3 is the confining pressure.

peak stress and strain rate, a linear function is used to fit the data under constant confining pressure. The fitting equations and relevant parameters are shown in Appendix 7.

To study the sensitivity of peak stress on the strain rate under dynamic compression, the typical hard rocks (Huashan granite and Linli sandstone)

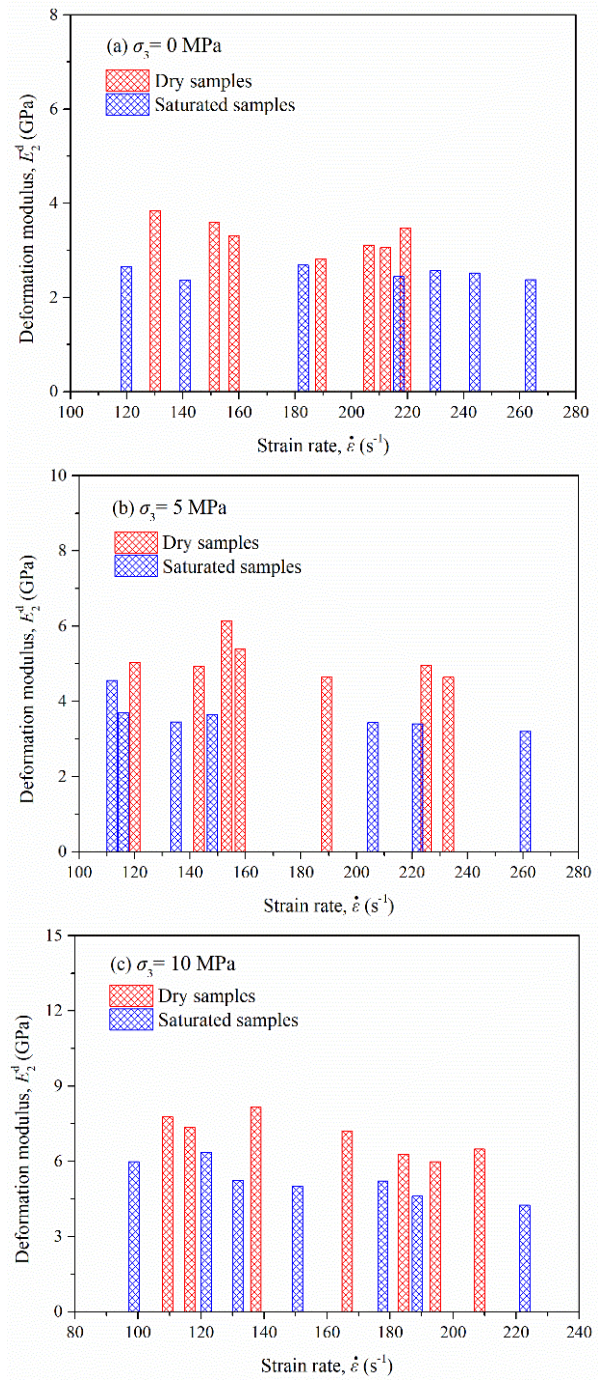


Figure 9 Relationship between dynamic deformation modulus (E_2^d) and strain rate. σ_3 is the confining pressure.

are compared with Sichuan schist in this paper. Figure 11 shows that the peak stresses of three kinds of rocks increase with increasing strain rate. There are good correlations between peak stresses and strain rates. However, the strain rate sensitivities of peak stresses are different under dynamic compression. The strain rate has the most

significant effect on the peak stress of Huashan granite (the slope of a fitted straight line is 1.85), followed by Linyi sandstone (the slope of a fitted straight line is 1.30) and Sichuan schist (the slope of a fitted straight line is 0.17). However, the peak stress of Linyi sandstone is the largest among the three kinds of rocks when the strain rates are approximately equal.

To study the sensitivity of peak stress on the confining pressure, herein, we compare and analyze the experimental data of granite, sandstone and schist. Figure 12 shows that the dynamic peak stresses of rocks increase linearly with the increase of confining pressure when the strain rates are approximately equal. The sensitivity of Linyi sandstone to the confining pressure is the most significant (the slope of a fitted straight line is 7.39), followed by Huashan granite (the slope of a fitted straight line is 5.81) and Sichuan schist (the slope of a fitted straight line is 4.99).

2.2 Failure mode analysis

The failure modes of schist under uniaxial impact tests are shown in Appendix 8. When the strain rate is low, the fracture surface develops along the axial direction (loading direction) and the rock fragment has a long strip shape. With increasing strain rate, the number of rock fragments increases. The failure modes of schist samples belong to typical axial tensile failure under uniaxial impact tests.

The failure modes of schist under triaxial impact tests are shown in Appendix 9. Shear failure is the main failure mode under triaxial impact tests. With increasing strain rate, fragments of schist also increase. Because of the restraining effect of confining pressure, the schist is only partially broken. As shown in Appendixes 8 and 9, the fragmentation degree of water-saturated schist is higher than that of dry schist. Hence, the ability of water-saturated schist to resist impacting is reduced.

Failure modes of saturated and dry schist under different confining pressures are shown in Appendix 10. When the confining pressure is zero (uniaxial impact test), the failure modes belong to tensile failure. When the confining pressures vary from 5 to 10 MPa, there is a certain angle between the fracture surface and axial direction. The failure

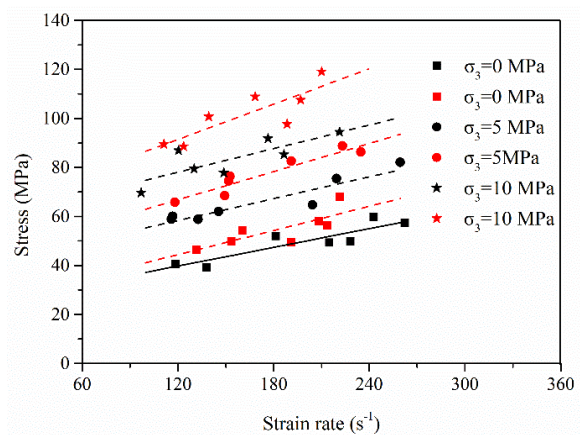


Figure 10 Relationship between dynamic peak stress and strain rate (Black denotes water-saturated schist and Red denotes dry schist). σ_3 is the confining pressure.

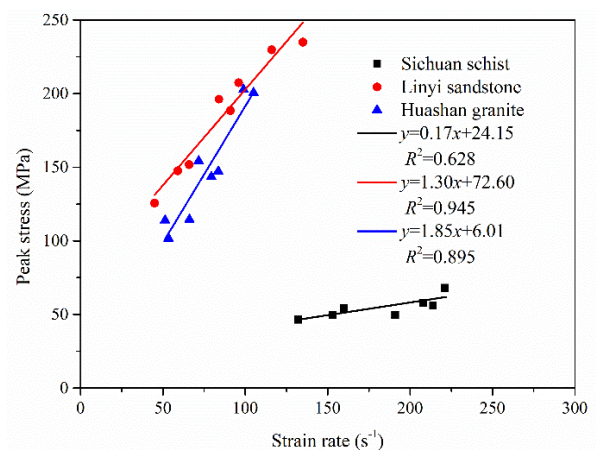


Figure 11 Relationship between dynamic peak stress and strain rate under uniaxial compression (The data of Huashan granite and Linyi sandstone are from Wang et al. (2018) and Gong et al. (2019) respectively).

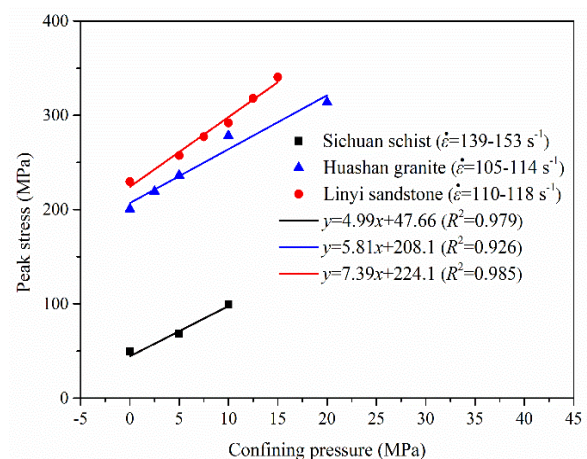


Figure 12 Relationship between dynamic peak stress and confining pressure (The data of Huashan granite and Linyi sandstone are from Wang et al. (2018) and Gong et al. (2019) respectively). $\dot{\epsilon}$ is the strain rate.

modes are shear failure. This implies that the failure modes of schist change from tensile failure to shear failure with the increase of confining pressure.

2.3 Static test results

After a series of static triaxial compression tests, the static mechanical properties of schist were revealed (Appendix 11). The static stress-strain curves of saturated and dry schist are shown in Figure 13. The static stress-strain curves of schist under different confining pressures include initial compaction, elastic, yield, and failure stages. Figure 13 demonstrates that the peak stress of schist increases gradually with the increase in confining pressure. Compared with the dry schist, the peak stress and deformation modulus of saturated schist clearly decrease. When the confining pressures are the same, the peak strain of water-saturated schist is greater than that of dry schist. Furthermore, compared with the dynamic test results, the static peak stresses are smaller than dynamic ones. However, the peak strain shows no clear tendency.

3 Discussion

To analyze the strain rate effects of dry and saturated schist, the dynamic increasing factor (DIF) is introduced (Zhou et al. 2012; Xia and Yao 2015):

$$DIF = \frac{\sigma_d}{\sigma_s} \quad (6)$$

where σ_d is the dynamic peak stress; and σ_s is the static peak stress.

For convenience, herein, the dynamic peak stresses under nine strain rates (100, 120, 140, 160, 180, 200, 220, 240 and 260 s⁻¹, respectively) are calculated according to the fitting formulas (Appendix 7). The static peak stresses under different confining pressures are calculated according to the fitting formulas (Appendix 12). The corresponding DIFs are calculated according to Eq. (6). As shown in Figure 14, DIFs of saturated schist are higher than those of dry schist. DIF differences between saturated schist and dry schist increase with increasing strain rate. For example, under uniaxial dynamic tests (Figure 14a) with a

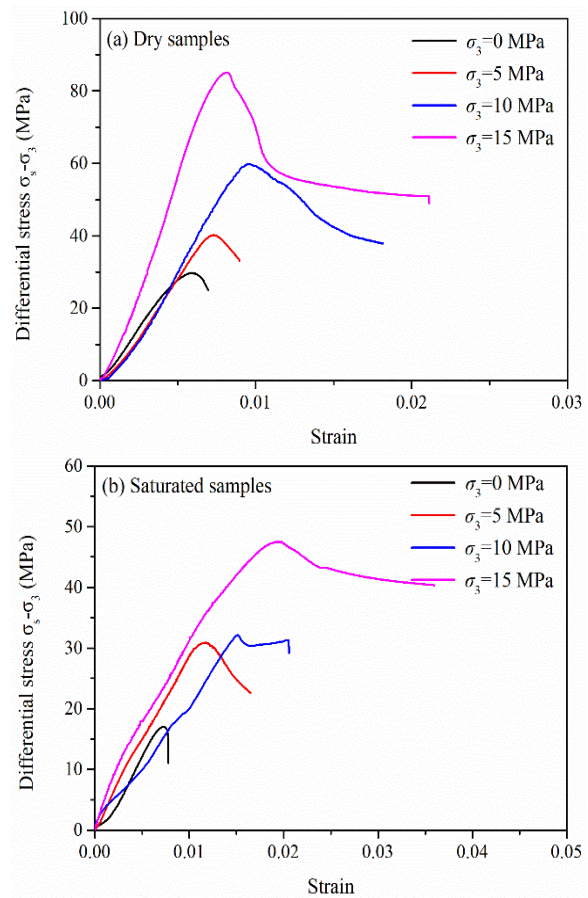


Figure 13 Static stress-strain curves: (a) Dry samples; (b) Saturated samples. σ_3 is the confining pressure; σ_s is the static peak stress.

strain rate of 100 s⁻¹, DIFs of dry and saturated schist amount to 1.58 and 2.06, respectively. The DIF difference is 0.48. When the strain rate increases to 260 s⁻¹, DIFs of dry and saturated schist amount to 2.61 and 3.21, respectively. The DIF difference is 0.60. This implies that the strain rate effect of schist is enhanced by fissure water, and the influence increases with the increase of strain rate.

When the confining pressure increases to 5 MPa (the strain rate is 100 s⁻¹), DIFs of dry and saturated schist amount to 1.27 and 1.72, respectively (Figure 14b), whereas the DIF difference is 0.45. Continually, when the strain rate increases to 260 s⁻¹, DIFs of dry and saturated schist amount to 1.90 and 2.47, respectively, whereas the DIF difference is 0.57. With the increase of confining pressure, the DIFs and DIF differences decreased gradually. This indicates that confining pressure can weaken the strain rate effect of peak stress. Compared with dry schist, the strain

rate effect of saturated schist is more sensitive to confining pressure.

Although the strain rate effect of schist is enhanced by water, the dynamic peak stress of saturated schist is still lower than that of dry schist in this paper. The test results of our study are different from previous studies (Lou 1994; Yuan and Ma 2015; Zhou et al. 2016; Gao et al. 2018). The dynamic peak stress of saturated schist is different from hard rock. Compared with hard rock, the softening effect of water on schist is more significant. In fact, water has dual effects on the dynamic peak stress of schist.

3.1 Degradation mechanism of water-saturated schist

There is a considerable amount of clay minerals and quartz particles in schist. During the saturation process, a large number of water molecules are adsorbed on the surface of clay particles, which leads to swelling and deformation of clay minerals (Anderson et al. 2009; Hensen and Smit 2012). As shown in Figure 15, the surface of a clay mineral is flat and smooth (Figure 15a). The boundaries of mineral particles are clear. Because of the swelling and softening of clay minerals during the saturation process, the boundaries between mineral particles become blurred (Figure 15b). The mineral structure tends to be loose and porous, which leads to the decrease of cohesion and strength. In addition to swelling and deformation of clay minerals, the chemical reaction cannot be ignored, which further reduces the strength of schist. In addition, the hydrolysis of Si-O-Si bond is also an important factor for the degradation of mechanical property. Schist consists of many quartz minerals (32%). During the saturation process, the cracks are full of free water. The crack tip is the most active area of water-rock reaction (Newman 1983). Owing to hydrolysis reaction, the strong Si-O-Si bond is replaced by the weak Si-OH bond (Cadoni et al. 2001), which reduces the growth barrier and fracture toughness of micro-cracks. The strength of schist is further reduced. The hydrolysis reaction formula can be expressed as

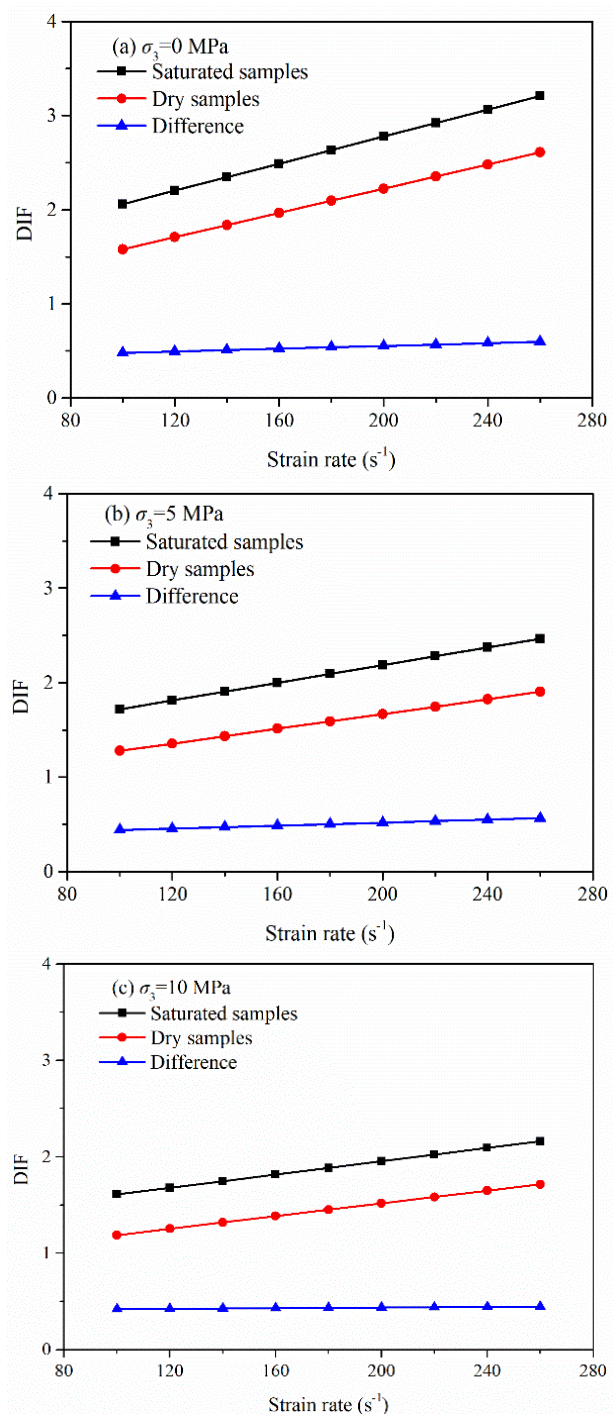
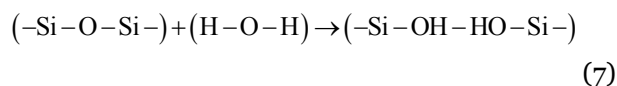


Figure 14 Variation of dynamic increasing factor (DIF) with increasing strain rate: (a) $\sigma_3 = 0$ MPa; (b) $\sigma_3 = 5$ MPa; (c) $\sigma_3 = 10$ MPa. σ_3 is the confining pressure.

3.2 Water-enhancing mechanism for the dynamic peak stress of schist

DIFs of saturated schist are higher than those of dry schist. DIF differences between saturated

schist and dry schist increase with increasing strain rate. This shows that the strain rate effect of schist is enhanced by fissure water, and the influence increases with the increase of strain rate. This may be explained by the viscous effect of fissure water. To study the influence of water on crack propagation, the sliding crack model is adopted to analyze the propagation of single crack under triaxial impact tests. The interaction between cracks is not considered. At first the initial main crack propagates along the original direction under triaxial impact test. With the increase of dynamic load, the main crack tip begins to produce large tensile stress. According to fracture mechanics,

when the stress intensity factor at the crack tip exceeds the fracture toughness of the matrix, the main crack will bend. The wing cracks begin to appear at both ends of the main crack (Figure 16).

Under impact loading, crack growth mainly includes shear slipping of the main crack and tensile opening of the wing crack. When the main crack slides, fissure water will produce the viscous force (τ_v) according to the law of Newton inner friction, which can be approximately expressed as (Wang et al. 2018)

$$\tau_v = \eta \frac{v}{h} \tag{8}$$

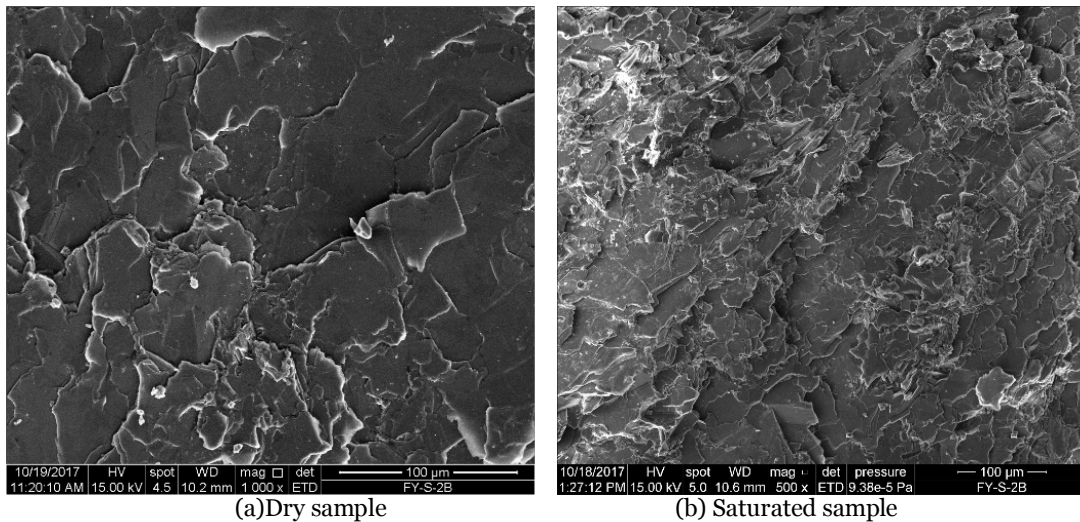


Figure 15 Scanning electron microscope(SEM) photographs of schist.

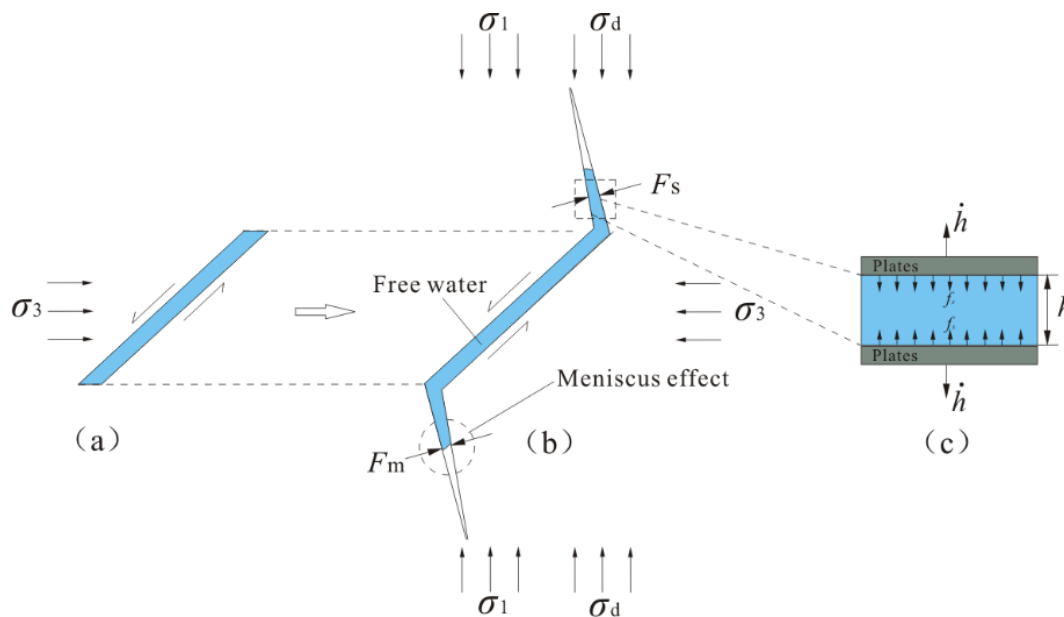


Figure 16 Sliding crack model: (a) Main crack; (b) Wing crack growth; (c) Stefan effect.

where η is the viscosity of liquid; h is the thickness of liquid; and v is slip rate of fracture.

When the wing crack opens, because of the Stefan effect, the viscous force (F_s) is formed on the crack surface, which hinders the propagation of the wing crack. In addition, previous studies have shown that the crack growth rate is much lower than loading rate under impact loading. The free water in main crack cannot reach the tip of wing crack in time (Rossi 1991; Rossi et al. 1992). The free water in wing crack will produce the meniscus. Owing to the Meniscus effect, the viscous force (F_m) is formed on the surface of wing crack, which prevents its growth. The formulas can be expressed as (Rossi 1991; Rossi et al. 1992; Zhang and Li 2004)

$$F_s = \frac{3\pi\eta r^4}{2h^3} \frac{dh}{dt} \quad (9)$$

$$F_m = \frac{\gamma V}{2r_c^2 \cos\theta} \quad (10)$$

where η is the viscosity of liquid; h is the thickness of liquid; r is the radius of the equivalent plate; dh/dt is the relative velocity of two plates; γ is the surface energy of liquid; θ is the wetting angle of the meniscus; r_c is the curvature radius of the meniscus; and V is the volume of liquid.

According to Eqs. (8) - (10), the viscous force produced by fissure water is affected by the water content, the geometric size of crack, and the rate of crack propagation. When the crack size and water content are constant, the viscous force increases with the increase in the crack growth rate. According to fracture mechanics, the crack growth rate is proportional to the loading rate. Therefore, the viscous force increases with the increase of the loading rate. Because of the viscous force of fissure water, the crack propagation is restrained. Therefore, water-saturated schist has higher strain rate effect compared with dry schist.

The analysis above shows that water has dual effects on the dynamic peak stress of schist. On the one hand, water-rock interaction changes the contact relation between the mineral particles and reduces fracture toughness of crack. This leads to the decrease in peak stress. On the other hand, under impact loading, fissure water will produce the viscous force, which hinders the crack propagation. This leads to the increase in peak stress. In this study, when strain rate varies from 96 to 262 s⁻¹, the water-rock interaction is

dominant. The dynamic peak stress of saturated schist is lower than that of dry schist. However, with the increase of strain rate, the viscous effect of fissure water will exceed the water-rock interaction. Consequently, the dynamic peak stress of saturated schist will be further improved. In addition, because of the confining pressure effect, the crack growth rate and the viscous effect of fissure water decrease. Therefore, compared with dry schist, dynamic peak stress of saturated schist is more sensitive to the confining pressure.

4 Conclusions

In this study, we have carried out a series of triaxial impact tests on dry and water-saturated schist by employing a modified triaxial SHPB system. We also conducted the static triaxial compression tests of schist for comparison. Furthermore, we have analyzed the impact deformation, peak stress, and failure mode of schist under triaxial stress restraint. The strain rate effects of dry and water-saturated schist were discussed and the dynamic response mechanism of saturated schist was revealed. The main conclusions drawn from the results are presented as follows:

1. The schist is a type of water-sensitive rock; water has clear influence on its strength and deformation. The stress-strain curves of saturated schist show clear ductility. We find that the peak strain of schist increases with increasing strain rate. Furthermore, under a constant strain rate, deformation moduli increase with the increase of confining pressure. Compared with static test results, the dynamic peak stress of schist is improved significantly.
2. The confining pressure effect and strain rate effect are clearly observed for the peak stress of schist. Peak stress of schist increases with the increase of strain rate and confining pressure. Compared with granite and sandstone, the sensitivity of schist to the confining pressure and strain rate is decreased.
3. The strain rate effect of schist is enhanced by fissure water, and the influence increases with the increase of strain rate. Compared with dry schist, the strain rate effect of saturated schist is more sensitive to the confining pressure.

Furthermore, water has dual effects on the peak stress of schist. The peak stress is affected by the combined softening and viscous effects of water under impact loading.

4. The failure mode of schist sample belongs to axial tensile failure parallel to the loading direction under uniaxial impact tests. The shear failure is the main failure mode under triaxial impact tests. With the increase in confining pressure, the failure modes of schist change from tensile failure to shear failure.

Because of the limitations concerning test conditions, dynamic triaxial tests with higher strain rates and triaxial confining pressures were not carried out in this study. However, bearing in mind its conclusions, we believe that it would be beneficial that dynamic mechanical properties of

saturated soft rock with higher triaxial confining pressures and strain rates are further investigated.

Acknowledgements

This work was supported by the Fundamental Research Funds for the Central Universities, CHD (300102260708), the National Natural Science Foundation of China (No. 41831286) and the Transportation Construction Science and Technology Program of Sichuan Province (No. 2015A1-3).

Electronic supplementary material: Supplementary material (Appendixes 1~12) is available in the online version of this article at <https://doi.org/10.1007/s11629-019-5900-2>.

References

- Anderson RL, Ratcliffe I, Greenwell HC, et al. (2009) Clay swelling-A challenge in the oilfield. *Earth Science Reviews* 98 (4): 201-216. <https://doi.org/10.1016/j.earscirev.2009.11.003>
- Aydan O, Sato A, Yagi M (2014) The inference of geo-mechanical properties of soft rocks and their degradation from needle penetration tests. *Rock Mechanics and Rock Engineering* 47(5): 1867-1890. <https://doi.org/10.1007/s00603-013-0477-5>
- Cadoni E, Labibes K, Albertini C, et al. (2001) Strain-rate effect on the tensile behavior of concrete at different relative humidity levels. *Materials and Structures* 34: 21-26. <https://doi.org/10.1617/13528>
- Chen YL, Wu P, Yu Q, et al. (2017) Effects of freezing and thawing cycle on mechanical properties and stability of soft rock slope. *Advances in Materials Science and Engineering Article* 2017: 1-10. <https://doi.org/10.1155/2017/3173659>
- Erguler ZA, Ulusay R (2009) Water-induced variations in mechanical properties of clay-bearing rocks. *International Journal of Rock Mechanics and Mining Sciences* 46(2): 355-370. <https://doi.org/10.1016/j.ijrmmms.2008.07.002>
- Gong FQ, Li XB, Liu XL (2011) Preliminary experimental study of characteristics of rock subjected to 3D coupled static and dynamic loads. *Chinese Journal of Rock Mechanics and Engineering* 30(6): 1179-1190. (In Chinese).
- Galindo RA, Serrano A, Olalla C (2017) Ultimate bearing capacity of rock masses based on modified Mohr-Coulomb strength criterion. *International Journal of Rock Mechanics and Mining Sciences* 93:215-225. <https://doi.org/10.1016/j.ijrmmms.2016.12.017>
- Gao LS, Xu Y, Wu BB, et al. (2018) Dynamic compression strength of thermal damaged Fangshan marble on dry and saturated conditions. *Chinese Journal of Rock Mechanics and Engineering* 37(S2): 3826-3833. (In Chinese). <https://doi.org/10.13722/j.cnki.jrme.2018.0642>
- Gong FQ, Si XF, Li XB, et al. (2019) Dynamic triaxial compression tests on sandstone at high strain rates and low confining pressures with split Hopkinson pressure bar. *International Journal of Rock Mechanics and Mining Sciences* 113: 211-219. <https://doi.org/10.1016/j.ijrmmms.2018.12.005>
- He MC, Xie HP, Peng SP, et al. (2005) Study on rock mechanics in deep mining engineering. *Chinese Journal of Rock Mechanics and Engineering* 24(16): 2803-2813. (In Chinese).
- Huang S, Xia K, Yan F, et al. (2010) An experimental study of the rate dependence of tensile strength softening of Longyou sandstone. *Rock Mechanics and Rock Engineering* 43(6): 677-683. <https://doi.org/10.1007/s00603-010-0083-8>
- Hensen EJM, Smit B (2012) Why clays swell. *Journal of Physical Chemistry B* 106(49): 12664-12667. <https://doi.org/10.1021/jpo264883>
- Karakul H, Ulusay R (2013) Empirical correlations for predicting strength properties of rocks from P-wave velocity under different degrees of saturation. *Rock Mechanics and Rock Engineering* 46(5): 981-999. <https://doi.org/10.1007/s00603-012-0353-8>
- Lou WT (1994) Dynamic fracture behavior of dry and waterlogged granite. *Explosion and Shock Waves* 14(3): 249-254. (In Chinese).
- Li XB, Lou TS, Zhao J (2005) Dynamic characteristics of granite subjected to intermediate loading rate. *Rock Mechanics and Rock Engineering* 38(1): 21-39. <https://doi.org/10.1007/s00603-004-0030-7>
- Li XB, Zou Y, Zhou ZL (2014) Numerical simulation of the rock SHPB test with a special shape striker based on the discrete element method. *Rock Mechanics and Rock Engineering* 47(5): 1693-1709. <https://doi.org/10.1007/s00603-013-0484-6>
- Newman GH (1983) The effect of water chemistry on the laboratory compression and permeability characteristics of some North Sea Chalks. *Journal of Petroleum Technology* 35: 976-980. <https://doi.org/10.2118/10203-PA>
- Petrov YV, Smirnov IV, Volkov GA, et al. (2017) Dynamic failure of dry and fully saturated limestone samples based on incubation time concept. *Journal of Rock Mechanics and Geotechnical Engineering* 9(1): 125-134.
- Rossi P (1991) A physical phenomenon which can explain the mechanical behavior of concrete under high strain rates. *Materials and Structures* 24: 422-424. <https://doi.org/10.1007/BF02472015>
- Rossi P, Vanmier JGM, Boulay C (1992) The dynamic behavior of concrete: influence of free water. *Materials and Structures* 25(9): 509-514. <https://doi.org/10.1007/BF02472446>
- Roy DG, Singh TN, Kodikara J (2017) Effect of water saturation on the fracture and mechanical properties of sedimentary rocks. *Rock Mechanics and Rock Engineering* 50(10): 2585-

2600. <https://doi.org/10.1007/s00603-017-1253-8>
- Vásárhelyi B, Ván P (2006) Influence of water content on the strength of rock. *Engineering Geology* 84(1-2): 70-74. <https://doi.org/10.1016/j.enggeo.2005.11.011>
- Wang B, Li X, Yin T, et al. (2010) Split Hopkinson pressure bar (SHPB) experiments on dynamic strength of water-saturated sandstone. *Chinese Journal of Rock Mechanics and Engineering* 29: 1003-1009.
- Wu ZJ, Wong LNY (2012) Frictional crack initiation and propagation analysis using the numerical manifold method. *Computers and Geotechnics* 39: 38-53. <https://doi.org/10.1016/j.compgeo.2011.08.011>
- Wong LNY, Maruvanchery V, Liu G (2016) Water effects on rock strength and stiffness degradation. *Acta Geotechnica* 11(4): 713-737. <https://doi.org/10.1007/s11440-015-0407-7>
- Wolfs RJM, Bos FP, Salet TAM (2018) Early age mechanical behavior of 3D printed concrete: Numerical modeling and experimental testing. *Cement and Concrete Research* 106: 103-116. <https://doi.org/10.1016/j.cemconres.2018.02.001>
- Wang JL, Zhang JX, Ren XH (2018) Stability analysis of chlorite schist surrounding rock based on parameters reduction. *Journal of China Three Gorges University* 40(1): 34-42. (In Chinese). <https://doi.org/10.13393/j.cnki.issn.1672-948X.2018.01.008>
- Wang ZL, Li HR, Wang JG (2018) Experimental study on mechanical and energy properties of granite under dynamic triaxial condition. *Geotechnical Testing Journal* 41(6): 1063-1075. <https://doi.org/10.1520/GTJ20170237>
- Xia K, Yao W (2015) Dynamic rock tests using split Hopkinson bar system-A review. *Journal of Rock Mechanics and Geotechnical Engineering* 7(1): 27-59. <https://doi.org/10.1016/j.jrmge.2014.07.008>
- Yuan P, Ma RQ (2015) Split Hopkinson pressure bar tests and analysis coalmine sandstone with various moisture contents. *Chinese Journal of Rock Mechanics and Engineering* 34: 2888-2893. (In Chinese). <https://doi.org/10.13722/j.cnki.jrme.2014.0534>
- Zhou ZL, Li XB, Liu AH (2011) Stress uniformity of split Hopkinson pressure bar under half-sine wave loads. *International Journal of Rock Mechanics and Mining Sciences* 48(4): 697-701. <https://doi.org/10.1016/j.ijrmms.2010.09.006>
- Zhou YX, Xia K, Li XB (2012) Suggested methods for determining the dynamic strength parameters and Mode-I fracture toughness of rock materials. *International Journal of Rock Mechanics and Mining Sciences* 49: 105-112. <https://doi.org/10.1016/j.ijrmms.2011.10.004>
- Zhang QB, Zhao J (2014) A review of dynamic experimental techniques and mechanical behavior of rock materials. *Rock Mechanics and Rock Engineering* 47(4): 1411-1478. <https://doi.org/10.1007/s00603-013-0463-y>
- Zhou ZL, Cai X, Zhao Y (2016) Strength characteristics of dry and saturated rock at different strain rates. *Transactions of Nonferrous Metals Society of China* 26(7):1919-1925. [https://doi.org/10.1016/S1003-6326\(16\)64314-5](https://doi.org/10.1016/S1003-6326(16)64314-5)
- Zhou ZL, Cai X, Ma D, et al (2018) Dynamic tensile properties of sandstone subjected to wetting and drying cycles. *Construction and Building Materials* 182: 215-232. <https://doi.org/10.1016/j.conbuildmat.2018.06.056>
- Zhou ZL, Cai X, Ma D (2019) Water saturation effects on dynamic fracture behavior of sandstone. *International Journal of Rock Mechanics and Mining Sciences* 114: 46-61. <https://doi.org/10.1016/j.ijrmms.2018.12.014>